

Electron-acoustic-phonon interaction in core/shell Ge/Si and Si/Ge nanowires

Darío G. Santiago-Pérez,^{1,2} C. Trallero-Giner,³ and G. E. Marques⁴

¹*Universidad de Sancti Spiritus “José Martí Pérez”, Ave. de los Mártires 360, CP 62100, Sancti Spiritus, Cuba*

²*CLAF - Centro Latino-Americano de Física, Avenida Venceslau Braz, 71, Fundos, 22290-140, Rio de Janeiro, RJ, Brasil*

³*Department of Theoretical Physics, Havana University, Havana 10400, Cuba*

⁴*Departamento de Física, Universidade Federal de São Carlos, 13.565-905 São Carlos, Brazil*

(Dated: June 16, 2022)

General expressions for the electron- and hole-acoustical-phonon deformation potential Hamiltonian ($H_{E- DP}$) are derived for the case of Ge/Si and Si/Ge core/shell nanowire structures (NWs) with circular cross section. Based on the short-range elastic continuum approach and on derived analytical results, the spatial confined effects on the vector phonon displacement, the phonon dispersion relation and the electron- and hole-phonon scattering amplitudes are analyzed. It is shown that the acoustical vector displacement, phonon frequencies and $H_{E- DP}$ present mixed torsional, axial, and radial components depending on the angular momentum quantum number and phonon wavevector under consideration. The treatment shows that bulk group velocities of the constituent materials are renormalized due to the spatial confinement and intrinsic strain at the interface. The role of insulating shell on the phonon dispersion and electron-phonon coupling in Ge/Si and Si/Ge NWs are discussed.

PACS numbers: 62.23.Hj,63.20.D-,63.20.kd

I. INTRODUCTION

Based on enforcement of Si nanowires (NWs) linked to thermal conductivity,¹ photodetectors² and solar cells,³⁻⁵ nowadays a notable effort has been addressed to Si/Ge and Ge/Si core/shell semiconductor NWs.⁶⁻⁹ These novel structures have countless applications where typical type-II band alignment can be formed.¹⁰⁻¹² With a natural spatial separation between electrons and holes by the constituent materials and due to the band offset, higher mobility of carriers are reported.¹³ Also, it is well established that the band structure of the core/shell Si/Ge and Ge/Si nanostructures depend on the radius, increasing the gap at Γ -point with reducing the radius. An effect directly linked to the spatial confinement and to the intrinsic strain at the interface^{11,14} due to the lattice mismatch up to 4 % between Si and Ge. Moreover, the band gap depends on the crystalline orientation of the wire.¹⁵ In consequence, the Si/Ge and Ge/Si core/shell in nanoscale regime show a direct band gap at Γ .^{6,16,17}

In NWs, the bulk acoustic-phonon modes are altered due to the mismatch in the elastic properties of the constituents materials. An important aspect to be considered is the role of spatial confinement in modifying acoustic-phonon modes and electron-phonon interaction. If the radius of the quantum wire is of the order or smaller than the phonon wave length, the acoustic phonon dispersion is strongly modified.¹⁸ The confined acoustic phonon in such nanostructure plays an important role on the carrier scattering rate, flow of electric current, mobility or transport. Thus, the reduction of the thermal conductivity and the characteristic of the carrier mobility in core/shell NWs are directly linked to the confined effects on the phonon dispersion relation.¹⁹⁻²² It is impor-

tant to remark that the core/shell wire structures provide useful optical applications^{23,24} and as quantum computer engineering for spin qubits.^{25,26}

Several works have been devoted to obtain the acoustic phonon dispersion in wires and core/shell nanowires using both *ab initio* calculations^{27,28} and phenomenological continuum approach (see Refs. 18, 29, and 30 and references there in). In addition, there have some effort to study the electron-phonon interaction for the conduction band³¹⁻³³ Despite the above, the electron-acoustic-phonon interaction in core-shell NWs has not been tackled entirely. A phenomenological theory, allowing the evaluation the electron-phonon Hamiltonian due to deformation potential interaction for cylindrical structure with arbitrary radii for both core and shell at the nanoscale regime, is a central issue for understanding the fundamental physics of many of the phenomena aforementioned. In the present work we study the electron-phonon interaction in Ge-core/Si-shell and Si-core/Ge-shell NWs in the framework of the continuum models and the $\vec{k} \cdot \vec{p}$ band theory.

This paper is organized as follows: In Sec. II we write the general expression for the electron- and hole- phonon deformation-potential Hamiltonians. For the conduction band we assume the Γ_{1c} symmetry valid for Ge/Si and Si/Ge NWs grown along [110], while for the holes we adopt the Bir-Pikus Hamiltonian (BPH) for states near the top of the valence bands with Γ_{15v} symmetry. A description of elastic continuum model and the general basis of solutions for the phonon amplitudes are devoted in Sec. III. We emphasize the phonon spectrum calculations, the role of the spatial confinement effect, the symmetry of the space of solutions and the homogeneous wire limit. In Sec. IV, we present a detailed derivation of the electronic-acoustic phonon scattering rate for conduction

and valence bands. We present the variation of the scattering amplitude with core and shell radii for electrons and holes interacting with the confined phonon. We discuss the influence of the geometry with respect to the homogeneous wire. We report our main results in Sec. V. Finally, in the Appendixes we summarize the most relevant elements in the development of the work.

II. ELECTRON-ACOUSTIC-PHONON INTERACTION

We consider typical core/shell cylindrical NWs with core radius r_c , shell thickness $\Delta = r_s - r_c$ and the z -axis parallel to the grown direction [110]. We assume that all involved parameters in the present theoretical model are piece-wise functions of r , i.e. we assumed isotropic parameters of the constituent materials.

In the occupation number representation the Hamiltonian of the electronic states interacting with the acoustic phonons can be expressed as³⁴

$$H_{e-ph} = \sum_{\alpha',\alpha} M_{\alpha',\alpha} \left[a_j^\dagger(\mathbf{k}_z) + a_j(-\mathbf{k}_z) \right] c_{\alpha'}^\dagger c_\alpha, \quad (1)$$

where $a_j^\dagger(\mathbf{k}_z)$ ($a_j(-\mathbf{k}_z)$) denotes the phonon creation (annihilation) operator in the j -branch with wavevector \mathbf{k}_z ($-\mathbf{k}_z$) and $c_{\alpha'}^\dagger$ (c_α) the corresponding electronic state α' (α). Here, $M_{\alpha',\alpha}$ takes into account the scattering event between the electronic states $\alpha \rightarrow \alpha'$ by the interaction with an acoustic phonon. It is well known that in Si and Ge semiconductors the electron-phonon coupling is determined by short range deformation-potential (DP) model.³⁵ In a first approach we develop a theory where this interaction is treated in the same way as the bulk DP approach. Nevertheless, it is reported that the DP constants are anisotropic and depend on the spatial confinement (see Ref. 4 and reference there in). The DP mechanism can be treated as a perturbation of the band energies due to the lattice distortion, in consequence the electron-phonon coupling depend on the electronic band structure.³⁵ As we stated above, the Ge/Si and Si/Ge core/shell nanowires grown [110] direction, show a direct band gap at Γ point of the Brillouin zone.^{16,17,36,37} Hence, the conduction band minimum shows Γ_{1c} , while the maximum valence band has Γ_{15v} symmetries, respectively.

A. Conduction band

Following the above discussion the electron-phonon scattering amplitude probability can be cast as

$$M_{\alpha'_e,\alpha_e} = \langle \Psi_{\alpha'_e} | a(\Gamma_{1c}) \nabla \cdot \mathbf{u} | \Psi_{\alpha_e} \rangle, \quad (2)$$

where $a(\Gamma_{1c})$ is the volume deformation potential,³⁵ \mathbf{u} is the vector phonon amplitude in the branch j and Ψ_{α_e} is the electron wave function for the core/shell NWs.

B. Valence band

For the scattering amplitude, $M_{\alpha'_h,\alpha_h}$, of a hole in the valence band interacting with an acoustic phonon we have

$$M_{\alpha'_h,\alpha_h} = \langle \Psi_{\alpha'_h} | H_{BP} | \Psi_{\alpha_h} \rangle, \quad (3)$$

where $|\Psi_{\alpha_h}\rangle$ is the hole wave function in the NW and H_{BP} is the Bir-Pikus Hamiltonian for the $J = 3/2$ valence bands states.^{35,38} Assuming the zinc-blende symmetry, the H_{BP} Hamiltonian in cylindrical coordinates and in the framework of the axial approximation can be written as

$$H_{BP} = \left[a(\Gamma_{15v}) - \frac{1}{2} b(\Gamma_{15v}) (J_z^2 - J^2/3) \right] \nabla \cdot \mathbf{u} + b(\Gamma_{15v}) \left[\frac{1}{2} J_\mp^2 \mathcal{X}^\pm + \sqrt{2} \{J_\mp, J_z\} \mathcal{Y}^\pm + \frac{3}{2} (J_z^2 - J^2/3) \varepsilon_{zz} \right], \quad (4)$$

with $a(\Gamma_{15v})$ and $b(\Gamma_{15v})$ the volume and shear deformation potentials for the highest energy Γ_{15v} valence band, respectively,³⁹ $\mathcal{X}^\pm = e^{\pm 2i\theta} (\varepsilon_{rr} - \varepsilon_{\theta\theta} \pm 2i\varepsilon_{r\theta})$, $\mathcal{Y}^\pm = e^{\pm i\theta} (\varepsilon_{rz} \pm i\varepsilon_{\theta z})$, $\{J_\mp, J_z\} = \frac{1}{2} (J_\mp J_z + J_z J_\mp)$, $J_\pm = (J_x \pm iJ_y)/\sqrt{2}$, being J_i the Cartesian angular-momentum operators for a particle with spin 3/2 and ε_{ij} the component of the stress tensor (see Appendix A Eq. (A2)).

III. ACOUSTIC-PHONON DISPERSION

For an evaluation of the Hamiltonian (1), and in consequence the matrix elements (2) and (3), it is necessary to knowledge the dependence of the phonon amplitude \mathbf{u} as well as the phonon frequencies on the core/shell spatial symmetry. In the framework of elastic continuum approach the equations of motion for the acoustical phonon modes takes the form⁴⁰

$$\rho \omega^2 \mathbf{u} - \nabla \cdot \sigma = 0, \quad (5)$$

with ρ the mass density, ω the phonon frequency and σ the mechanical stress tensor. Following the Hooke's law $\sigma = \mathbf{C} \cdot \varepsilon$, with ε the strain tensor and \mathbf{C} the elastic stiffness tensor (see Appendix A). Following the results compiled in the Appendix (A), the equation of motion for the acoustical phonon takes the form

$$\rho \omega^2 \mathbf{u} = \nabla(\rho v_L^2 \nabla \cdot \mathbf{u}) + \nabla \times (\rho v_T^2 \nabla \times \mathbf{u}). \quad (6)$$

The systems under consideration are inhomogeneous and the parameters in Eqs. (5) and (6) depend on the position coordinate r . The solution of (6) consists of a longitudinal (L) \mathbf{u}_L and two transverses (T) $\mathbf{u}_{T_1}, \mathbf{u}_{T_2}$

fields, i.e. $\mathbf{u} = \mathbf{u}_L + \mathbf{u}_{T_1} + \mathbf{u}_{T_2}$. Since the system is inhomogeneous, in general \mathbf{u}_L , \mathbf{u}_{T_1} , \mathbf{u}_{T_2} are coupled by the matching boundary conditions at the interface. Thus, the acoustic dispersion relations for the L and T branches are not independent and the normal modes become a hybrid of L , T_1 and T_2 phonon vibrational motions.

In cylindrical geometry, the solution of Eq. (6) has full axial symmetry, hence the vector amplitude in cylindrical coordinates can be cast as $\mathbf{u} = (u_r, u_\theta, u_z) \exp i(n\theta + k_z z)$. In consequence and following the method of solution described in Refs. 41 and 42, one can derive a general basis of solutions for (u_r, u_θ, u_z) , namely

$$\begin{pmatrix} u_r \\ u_\theta \\ u_z \end{pmatrix} = A_L \begin{pmatrix} q_L r_c f_n'(q_L r) \\ i \frac{nr_c}{r} f_n(q_L r) \\ ik_z r_c f_n(q_L r) \end{pmatrix} + A_{T_1} \begin{pmatrix} k_z r_c f_n'(q_T r) \\ i \frac{nk_z r_c}{r q_T} f_n(q_T r) \\ -iq_T r_c f_n(q_T r) \end{pmatrix} + A_{T_2} \begin{pmatrix} \frac{nr_c}{r} f_n(q_T r) \\ iq_T r_c f_n'(q_T r) \\ 0 \end{pmatrix}, \quad (7)$$

where $n = 0, \pm 1, \pm 2, \dots$ label the azimuthal motion, k_z is the z -component of the phonon wavevector, and $q_L(q_T)$ is given by

$$q_L^2(q_T^2) = \frac{\omega^2}{v_L^2(v_T^2)} - k_z^2. \quad (8)$$

In Eq. (7), if $x^2 > 0$ ($x^2 < 0$) the function $f_n(x)$ is taken as Bessel J_n (or Infeld I_n) for $0 \leq r \leq r_c$ and a linear combination of J_n and Neumann N_n functions of integer order n (or combination of $I_n(x)$ and MacDonald $K_n(x)$)⁴³ for $r_c \leq r \leq r_s$. From (7), it is easy to check that $\nabla \cdot \mathbf{u}_L = -(q_L^2 \pm k_z^2) A_L r_c f_n(q_L r) e^{i(n\theta + k_z z)}$ (sign + for the Bessel functions and - for the modified Bessel functions) and $\nabla \cdot \mathbf{u}_{T_1} = \nabla \cdot \mathbf{u}_{T_2} = \nabla \times \mathbf{u}_L = 0$, underlying the transverse and longitudinal character of the fields \mathbf{u}_{T_1} , \mathbf{u}_{T_2} and \mathbf{u}_L .

The eigenfrequencies of the phonon modes are obtained by imposing appropriate boundary conditions. We consider a free boundary at the shell surface, $\sigma \cdot \mathbf{e}_r|_{r_s} = 0$, besides, the mechanical displacement and the normal component of the stress tensor should be continuous at the core/shell interface, i.e. $\mathbf{u}|_{r_c^-} = \mathbf{u}|_{r_c^+}$ and $\sigma \cdot \mathbf{e}_r|_{r_c^-} = \sigma \cdot \mathbf{e}_r|_{r_c^+}$. Note that in the case of free standing homogeneous nanowires the space of solutions (7) match with those reported in Ref. 31.

The calculation for the acoustical modes in NWs with cylindrical symmetry is a complicate task. In general the phonon displacement \mathbf{u} has all three components (neither of the coefficients A_L , A_{T_1} and A_{T_2} is zero) and it cannot be decoupled into independent motions. For a given n , and k_z , the constants A_L , A_{T_1} and A_{T_2} are fully determined by the matching condition at $r = r_c$ and the boundary condition of free standing nanowires at $r = r_s$. Due to the cylindrical symmetry we cannot characterize

the modes as pure into torsional, dilatational and flexural modes. The resulting modes are a combination of transverse and longitudinal character. Nevertheless, from the symmetry of general basis (7) we are able obtain the following results: (i) for $n = 0$ and $k_z = 0$ we are in presence of three independent L , T_1 and T_2 uncoupled modes with amplitude $u_r(r)$, $u_z(r)$ and $u_\theta(r)$, respectively; (ii) for $n = 0$ and $k_z \neq 0$, the longitudinal and transverse T_1 motions, $L - T_1$, are coupled, while T_2 vibrational mode remains uncoupled; (iii) for $n \neq 0$ and $k_z = 0$, the T_1 transverse phonon is independent, while the other two, L and T_2 , are mixed; and finally, (iv) for $n \neq 0$ and $k_z \neq 0$ the longitudinal and the transverse T_1 and T_2 motions are coupled. Below, we focus on most relevant case of phonon with axial symmetry, ($n = 0$).

A. Phonons with $k_z = 0$

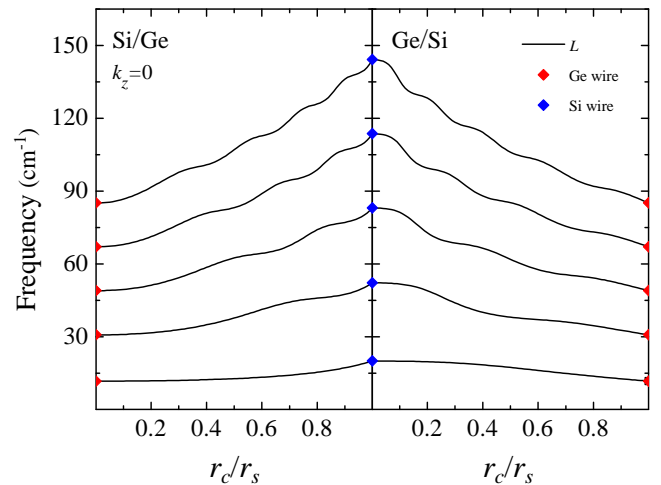


FIG. 1. (Color online) Frequencies of the first five breathing modes as a function of the ratio r_c/r_s for fixed shell radius $r_s = 5$ nm in Si/Ge (left panel) and Ge/Si (right panel) NWs grown along the [110] crystallographic direction. The limits of Ge and Si nanowires are shown by red and blue diamonds, respectively (see text).

As stated above, the present case shows three uncoupled vibrations, L , T_1 and T_2 . The longitudinal modes correspond to the radial breathing mode (RBM) and their eigenfrequencies are ruled by the secular equation

$$F_s(\gamma \lambda_L x) [G_s(\lambda_L x) J_1(x) - \rho_r F_c(x) N_1(\lambda_L x)] - G_s(\gamma \lambda_L x) [F_s(\lambda_L x) J_1(x) - \rho_r F_c(x) J_1(\lambda_L x)] = 0, \quad (9)$$

where c (s) labels the core (shell), $x = \omega r_c/v_{L_c}$ region, $\lambda_L = v_{L_c}/v_{L_s}$, $\gamma = r_s/r_c$, $\rho_r = \rho_s/\rho_c$, $F_i(x) = v_{L_i}^2 x J_0(x) - 2v_{T_i}^2 J_1(x)$, and $G_i(x) = v_{L_i}^2 x N_0(x) - 2v_{T_i}^2 N_1(x)$ ($i = s, c$). The RBM modes have been studied

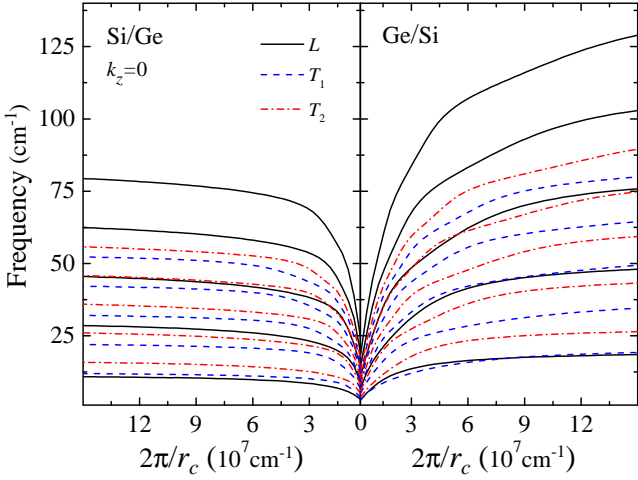


FIG. 2. (Color online) The same as Fig. 1 for the uncoupled L , T_1 and T_2 phonon modes as a function of $2\pi/r_c$, for fixed shell thickness $\Delta = r_s - r_c = 5$ nm.

in the past for both nanotubes^{44,45} and semiconductor NWs.^{46,47} Because of its particular relevance it becomes necessary to focus on these modes in Ge/Si and Si/Ge core/shell nanowires. It is expected that the frequencies of the RBM modes, which are described through the Eq. (9), are strongly dependent on the material composition, $\lambda_L = v_{L_c}/v_{L_s}$ and size ratio, $\gamma = r_s/r_c$. Firstly note from (9) that the two limiting cases $r_c = 0$ and $r_c/r_s = 1$ are provided by the secular equation $F_i(z_i) = 0$ with $z_i = \omega r_0/v_{L_i}$ ($i = s, c$) and r_0 the radius of the wire, i.e., the homogeneous NW dispersion relation is recovered for the shell or core semiconductors. Figure 1 shows the frequency dependence on the core/shell ratio r_c/r_s , the limiting cases of $r_c = 0$ and $r_c/r_s = 1$ are shown by diamonds. In the calculations we employed the following data for Si [Ge]: $v_L = 9.36$ [5.39] $\times 10^5$ cm/s, $v_T = 5.25$ [3.30] $\times 10^5$ cm/s,⁴⁸ $\rho = 2.33$ [5.32] g/cm³.⁴⁹ The observe oscillation in Fig. 1 of ω as function of the ratio r_c/r_s can be understood by the interference effect between shell and core structures. Thus, for small value of the ratio r_c/r_s the influence of the shell becomes stronger on the core phonon amplitude enhancing the number of oscillations. Moreover, the lower phonon frequencies is less affected showing almost a flat dispersion on r_c/r_s , while the higher excited modes are more sensitive with pronounced oscillations. The same trend is obtained for the T_1 and T_2 phonon modes (see Fig. 2).

The confined eigenfrequencies, $\omega(k_z = 0)$, for the T_2 mode can be obtained from the general expression

$$x_s J_1(x_c) P_{22}(x_s) + \frac{\rho_r}{\lambda_T^2} x_c J_2(x_c) P_{12}(x_s) = 0. \quad (10)$$

Here, $x_c[x_s] = r_c \sqrt{(\omega/v_{T_c}[v_{T_s}])^2 - k_z^2}$, $\lambda_T = v_{T_s}/v_{T_c}$ and $P_{n,m}(x) = J_n(x)N_m(\gamma x) - J_m(\gamma x)N_n(x)$. Also, in the particular case when $k_z = 0$ it is possible to get an explicit expression for the T_1 frequency mode.

Figure 2 displays the influence of the $2\pi/r_c$ on the uncoupled L , T_1 and T_2 phonon frequencies for fixed shell thickness $\Delta = r_s - r_c$. In the limit of $r_c \rightarrow \infty$ we recover the phonon frequency for the case of pure Si and Ge and wires. As $r_c \rightarrow \infty$ we have that the phonon frequency resembles the typical linear acoustic bulk phonon dispersion on the phonon wavevector. The spatial confinement renormalized the sound velocity and we can rewrite, for large values of r_c , that $\omega_{L,T}^{(j)} = (2\pi/r_c)v_{L,T}^{(j)}$ ($j = 1, 2, \dots$) with different slope $v_{L,T}^{(j)}$ for each mode. Notice that the cylindrical symmetry breaks the T_1 and T_2 degeneracy and we are in presence of two different sound velocities, $v_{T_1}^{(j)}$ and $v_{T_2}^{(j)}$.

B. Phonon dispersion with $k_z \neq 0$

Following the secular Eq. (10), in Fig. 3 we display the pure confined transverse T_2 phonon dispersion. For sake of comparison the bulk phonon dispersions, $\omega_{Ge}(k_z)$ and $\omega_{Si}(k_z)$, are represented by blue and red dashed lines, respectively. For small vales of k_z it is possible to get useful analytical solutions. It is important to remark that in the case of Ge/Si if the set of the values (ω, k_z) lies in the region $\omega_{Ge}(k_z) < \omega < \omega_{Si}(k_z)$, the parameter x_c is real while x_s becomes a complex number. For the Si/Ge NWs the opposite is obtained. Accordingly, for the Ge/Si we get that the function $P_{nm}(x_s) \Rightarrow P_{nm}(|x_s|) = I_n(|x_s|)K_m(\gamma|x_s|) - I_m(\gamma|x_s|)K_n(|x_s|)$.

The numerical solution of Eq. (10) shows a strong modification of the Si and Ge bulk phonon group velocities (see Fig. 3) which depend on the surrounding material, i.e. if the shell is composed of softer or harder material than the core semiconductor, the resulting group velocity have lower or higher values. For example, in Ge/Si core/shell NWs the shell compress the Ge core lattice while for Si/Ge the shell is compressed by the core and vice-versa. Similar result have been achieved in Ref. 18. To better visualize this dependence on the speed of sound on material parameters, from Eq. (10) and assuming small values of the wave number for k_z , follows the dispersion relation valid for Ge/Si (x_c real, x_s complex number) and Si/Ge (x_c complex number, x_s real)

$$\omega = v_{T_c} \sqrt{1 + \frac{(\lambda_T^2 - 1)(\gamma^4 - 1)\rho_r}{(\gamma^4 - 1)\rho_r + 1}} k_z = \bar{v}_T k_z. \quad (11)$$

The above equation shows that the lower mode presents a linear character in k_z with a renormalized sound velocity \bar{v}_T that takes into account the ratio of the shell and core radius, densities and transverse velocities. Equation (11) suggests the way to modify the sound velocity as a function of the geometric factors ranging between the values of v_T^{Ge} and v_T^{Si} .

In the domain of (ω, k_z) where x_c and x_s are both real functions, Eq. (10) provides for small values of k_z the dispersion relation

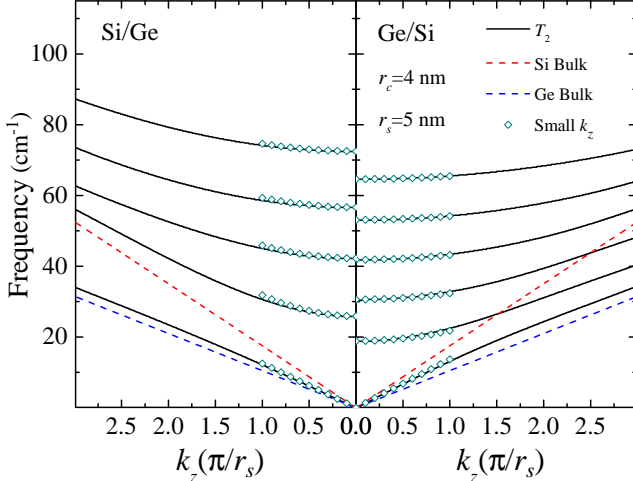


FIG. 3. (Color online) Phonon dispersion for the uncoupled T_2 modes as a function of the phonon wave vector k_z in units of π/r_s . Left panel Si/Ge; right panel Ge/Si NWs. Dashed lines represent the bulk dispersion relation for Si and Ge. Open diamonds are solutions of Eqs. (11) and (12).

$$\omega_{T_2}(k_z) = \omega_{T_2}(0) + \frac{1}{2} \frac{v_{T_s}^2}{\omega_{T_2}(0)} k_z^2, \quad (12)$$

where $\omega_{T_2}(0)$ is the confined phonon frequencies of the core/shell NWs for $k_z = 0$. In Fig. 3 the solutions given by Eqs. (11) and (12) are represented by open diamonds. By comparison with the numerical calculation of Eq. 10), it can be seen that explicit expressions (11) and (12) are good approximations for $k_z(\pi/r_s) \leq 1$.

Another subset of solutions corresponds to the hybridized longitudinal and transverse motions. Fig. 4 shows the phonon dispersion of the mixed $L - T_1$ modes for $\gamma = 1.25$. The longitudinal (L) and transverse (T_1) nomenclatures are taken from the character of the modes at $k_z = 0$. For sake of comparison the phonon dispersion for the homogeneous Si and Ge cylindrical wires are shown in Fig. 4. Here, the corresponding longitudinal and transverse modes are represented by red straight and red dash-dots lines, respectively. Due to the strain effect at the interface, it can be seen in the figure that for the Ge/Si core/shell NW the phonon frequencies lies below the pure Ge/ wire, while the opposite is obtained for the Si/Ge NW where ω_{Si} are well above of the core/shell Si/Ge phonon frequencies. At k_z approaching zero the lower mode presents a linear dependence of ω_{L-T_1} on the wave number k_z with certain effective sound velocity v_{L-T_1} that depend on the radius r_c and r_s . The bending appearing in the phonon dispersion at $\omega \sim 15 \text{ cm}^{-1}$ is a manifestation of the strongest coupling between L and T_1 modes. The mixed character of the states avoid crossing points in the phonon dispersion relation, i.e. a repulsion between near modes with the same symmetry occurs.

This effect is observed in all dispersion relations having an important consequence in the electron-phonon Hamiltonian H_{e-ph} (see discussion below). In Fig. 4 some anticrossings, associated with the mixing of L and T_1 states, have been indicated by full diamonds. The proximity of the levels bellowing to the same space of solution or with the same symmetry is avoided by the repulsion between the phonon states. At the anticrossings, a strong mixing of the L and T_1 states occurs and an exchange of the character of the constants A_L and A_{T_1} is obtained as a function of k_z .

Notice that the higher excited states for $k_z \sim 0$ do not present a strong mixing effect and the phonon dispersion relation can be described by simple parabolic law, $\omega_{L(T_1)}(k_z) = \omega_{L(T_1)}(0) + \beta_{L(T_1)}^2 k_z^2$. Here, $\beta_{L(T_1)}$ measures the curvature of the phonon dispersion and $\omega_{L-T_1}(0)$ is the NW phonon frequencies for $k_z = 0$. The same result we achieved for the homogeneous Si and Ge cylindrical wires.

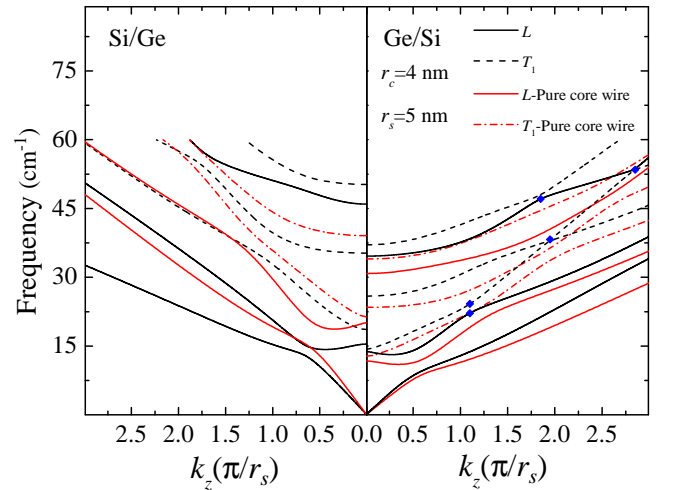


FIG. 4. (Color online) The same as Fig. 3 for the mixed $L - T_1$ modes. Phonon dispersion relations for homogeneous Si and Ge cylinder wires are represented by red straight (longitudinal modes) and dashed-dots (transversal modes) lines. Full diamonds represent the anticrossings between two nearby modes as explained in the text.

IV. SCATTERING RATE

Due to translational and cylindrical symmetries, the matrix element $M_{\alpha',\alpha}$ can be cast as following

$$M_{\alpha',\alpha} = S_{e-ph} \delta_{m',m+n} \delta_{k',k+k_z}, \quad (13)$$

where the angular momentum and momentum conservation are written explicitly. $S_{e-ph} = \langle m' | H_{e-ph} | m \rangle$ is the scattering amplitude due to the electronic transition assisted by an acoustical phonon between the electron or

hole states $|m'\rangle \rightarrow |m\rangle$ as given in the Appendixes B and C. We choose for the phonon eigenvectors $\{\mathbf{u}_{n,k_z}\}$ the normalization condition

$$\int \rho(r) |\mathbf{u}_{n,k_z}(\mathbf{r})|^2 dV = \frac{\hbar}{2\omega_n(k_z)}, \quad (14)$$

with $\omega_n(k_z)$ the acoustic-phonon dispersion of the core/shell problem. Let us discuss a general formulation for the electron-acoustic deformation potential Hamiltonian, $H_{E- DP}$ and an evaluation of the scattering amplitudes for the electrons and holes.

A. Electron-LA Hamiltonian

According to Eq. (2), the transverse or torsional mode does not induce volume change and only the longitudinal acoustic motion $\mathbf{u}_L(\mathbf{r})$, contributes to electron-phonon Hamiltonian, H_{E-DP} . Hence, and assuming in Eq. (7) A_L as independent constant, we have

$$H_{E-DP} = a(\Gamma_{1c}) \nabla \cdot \mathbf{u}_L = - \sqrt{\frac{\hbar\omega_n^3(k_z)}{4\pi r_c^2 L \rho_c v_L^4} \frac{a(\Gamma_{1c})}{\mathcal{N}_{n,k_z}}} f_n(q_L r) e^{i(n\theta + k_z z)}, \quad (15)$$

where $\mathcal{N}_{n,k_z} = \sqrt{\int_0^\gamma \rho(z) |\mathbf{u}_{n,k_z}(z)|^2 z dz / (\rho_c A_{Lc}^2)}$ is the normalization constant for the dimensionless phonon amplitude $\mathbf{u}_{n,k_z}(z)$.

In Fig. 5 the characteristic contour map for the electron-LA Hamiltonian (15) is shown for the Ge/Si NWs. We choose the first four modes of Fig. 4 where $\omega_{n=0}(k_z = 0) \neq 0$. According to the space of solution (7), for $n = 0$, the longitudinal waves \mathbf{u}_L , have non-zero radial and axial components. Figures 5 a), b), c) and d) correspond to the uncoupled confined frequencies $\omega_{LA}^{(1)}$, $\omega_{T_1}^{(1)}$, $\omega_{T_1}^{(2)}$, and $\omega_{LA}^{(2)}$ for $k_z = 0$ of the LA and T_1 motions. In the panels a) and d) we can observe that for $r = 0$ we have the stronger spatial localization in correspondence with the longitudinal character of these modes. In panel a), we observe that as the values of k_z increases the T_1 component becomes stronger and for $k_z > 1.1$ the contribution of the $\omega_{LA}^{(1)}$ mode to H_{E-DP} is almost zero. The same is observed in panel d) for the state $LA^{(2)}$ but the limit value is $k_z > 1.8$. These two values of k_z are in correspondence with the anticrossing shown by full diamonds in the Figure 4 for the $LA^{(1)}$ and $LA^{(2)}$ phonon states. Note in Fig. 4 that for $k_z \sim 2.8$ an anticrossing occurs and the $LA^{(2)}$ mode presents stronger LA character, and in consequence the spatial distribution of H_{E-DP} is enhanced. In panel b) the observed strong spatial localization of H_{E-DP} at $r = 0$ with $k_z \approx 0.2$ is explained by the reduction, in the state $T_1^{(1)}$, of the coefficient A_{T_1} as a function of k_z . Due to the anticrossing between the

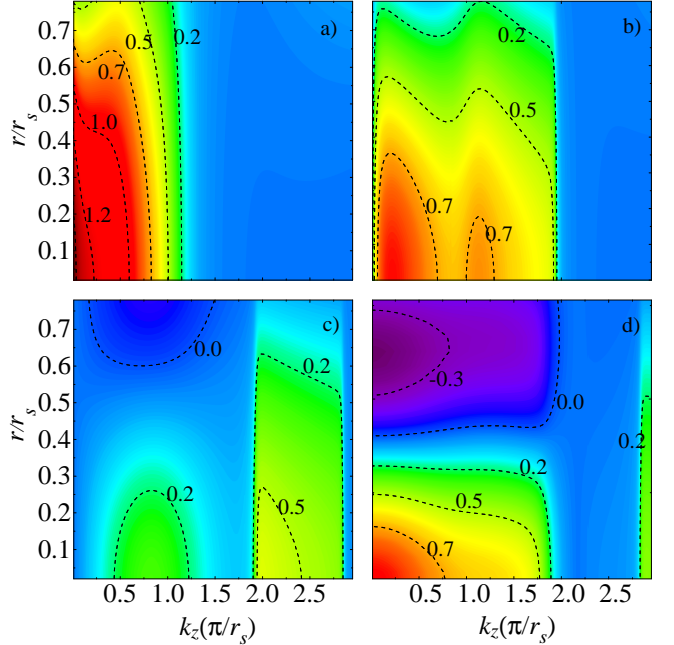


FIG. 5. (Color online) Contour plots of the Hamiltonian (15) in units of H_{OE} as function dimensionless wave number $k_z/(\pi/r_s)$ and radius r/r_c for the phonon modes a) $\omega_{LA}^{(1)}$, b) $\omega_{T_1}^{(1)}$, c) $\omega_{T_1}^{(2)}$, and d) $\omega_{LA}^{(2)}$ of the Ge/Si core/shell NW (see text). In the calculation we fixed $k_z = 0$ and $z = 0$.

states $T_1^{(1)}$ and $T_1^{(2)}$ for $k_z \approx 2$, the $\omega_{T_1}^{(1)}$ mode is almost transverse and its contribution to the spatial distribution $f_{n=0}(q_L r)|_{\omega=\omega_{T_1}^{(1)}}$ decay to zero. At the same time, the mode $T_1^{(2)}$ gains in the A_L amplitude, and H_{E-DP} at $\omega = \omega_{T_1}^{(2)}$ increases in the region $1.9 < k_z < 2.9$ as it is shown in Fig. 5c). Thus, the phonon dispersion of the Ge/Si NWs for a given ratio of r_s/r_c has a preponderant influence on the spatial distribution of H_{E-DP} as a function of the z -component of wavevector.

Taking into account the Eqs. (15), (B1) and (C2), the electron scattering amplitude can be written as

$$S_{E-DP} = \frac{1}{r_c^2} \langle F_{m'_e} | H_{OE} \frac{\omega_n}{v_L \mathcal{N}_{n,k_z}} f_n | F_{m_e} \rangle, \quad (16)$$

where $H_{OE} = -a(\Gamma_{1c}) \sqrt{\hbar\omega_{n=0}(k_z = 0) / 4\pi r_c^2 L \rho_c v_L^2}$. From Eq. (16) immediately follows that phonon modes with $n = 0$ assist to electron intrasubband transitions, $m'_e = m_e$, while for $n \neq 0$ we are in presence of intersubband transitions with $m'_e \neq m_e$.

Note that in the case of homogeneous wire $\langle F_{m'_e} | f_n | F_{m_e} \rangle / r_c^2$ corresponds to the electron form factor or overlap integral between the normalized radial electronic states and the phonon function f_n of the quantum wire. For sake of comparison we consider the Eq. (16) for a homogeneous wire. Assuming the size-quantum-

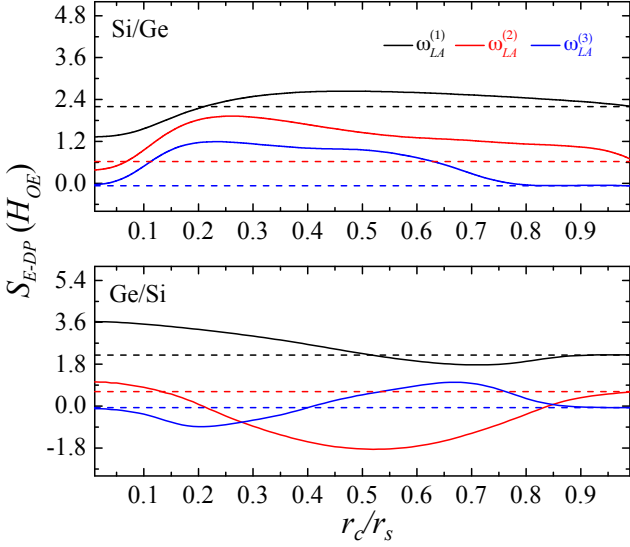


FIG. 6. (Color online) Electron scattering amplitude for the excited frequencies $\omega_{LA}^{(1)}$, $\omega_{LA}^{(2)}$ and $\omega_{LA}^{(3)}$ (see text) as a function of the ratio r_c/r_s . Dashed lines: homogeneous wires as given by Eq. (17). Upper panel Si/Ge, lower panel Ge/Si.

limit (strong spatial confinement) where electrons populate the lowest subband ($m'_e = m_e = 0$ and $n = 0$) and inter-subbands transitions $|p'_e\rangle \rightarrow |p_e\rangle$ are discarded, the scattering amplitude at $k_z = 0$ is reduced to

$$S_{E-DP}^H = H_{OE} \left(\frac{r_c^2 q_L^2}{4} \delta^4 - \delta^2 + 1 \right)^{-\frac{1}{2}} \times \frac{\langle J_0(p_e) | J_0(q_L) | J_0(p_e) \rangle}{r_c^2 J_1^2(p_e r_c) J_0(q_L r_c)}, \quad (17)$$

with $\delta = v_L/v_T$.

It is instructive to compare the behavior of the electron scattering amplitude S_{E-DP} in the case of core/shell Si/Ge and Ge/Si NWs. Fig. 6 displays the reduced scattering amplitude S_{E-DP}/H_{OE} as a function of the ratio r_c/r_s for both core/shell NWs. For H_{OE} we choose the parameters of Si or Ge semiconductor for Si/Ge and

Ge/Si NWs, respectively. For each structure, in the quantum limit approach the first three LA modes of the structure with frequencies $\omega_{LA}^{(j)}$ ($j = 1, 2, 3$) $\neq 0$ at $k_z = 0$ are considered. In the figure the form factor using Eq. (17) and $r_c = 5$ nm, is represented by dashed lines. In NWs of Si/Ge and Ge/Si the electrons are confined in the core and shell, respectively. For the evaluation of Eq. (16) we employed the results displayed in the Appendix B. In the upper panel of the Fig. 6 (Si/Ge NWs) is shown the influence of the shell of Ge on the S_{E-DP} . If $r_c = r_s$ we have a quantum wire of Si and S_{E-DP}/H_{OE} is described by Eq. (17). If $r_c/r_s \neq 1$ we are in presence of Si/Ge core/shell system. Thus, we can observe that the value of S_{E-DP} , for the $\omega_{LA}^{(1)}$ modes, firstly increases, reaching to a maximum (r_c/r_s)_{max}⁽¹⁾ ≈ 0.4 and for $\gamma < \gamma_{\max}^{(1)}$ the quantity S_{E-DP}/H_{OE} reaches asymptotically to the Si homogeneous wire value. In the case of $\omega_{LA}^{(j)}$ ($j = 2, 3$) the reduced scattering amplitude growths, reaching a maximum value near (r_c/r_s)_{max}⁽²⁾ ≈ 0.23 . For $\gamma < \gamma_{\max}^{(2)}$, S_{E-DP}/H_{OE} decreases to the limit value of Eq. (17). In the lower panel of Fig. 6 (Ge/Si NWs) the wire of Ge is reached at $r_c = r_s$. From the figure we can observe the strong influence of the shell on the S_{E-DP}^H for $r_c/r_s < 0.8$ and also the oscillations of S_{E-DP} around the S_{E-DP}^H values a fact reflecting the oscillator behavior of the phonon modes with γ (see Fig. 1). Similar result for the electron scattering amplitude has been reported in Ref. 50 for Si nanowires.

B. Hole-Acoustical-Phonon Hamiltonian

Employing the solutions for the phonon amplitude (7), the matrix representation of the angular momentum $J = 3/2$ ^{51,52} and the strain relations given in the Appendix A, the hole scattering amplitude for the Hamiltonian (4) can be cast as

$$S_{H-BP} = \left\langle \hat{F}_{m'_h}^{(i)} \right| H_{BP} \left| \hat{F}_{m_h}^{(i)} \right\rangle, \quad (18)$$

where $i = hh^+, lh^+, lh^-, hh^-$,

$$S_{H-BP} = \left\langle \begin{array}{c} a_{1i} F_{m_h+n} \\ a_{2i} F_{m_h+n+1} \\ a_{3i} F_{m_h+n+2} \\ a_{4i} F_{m_h+n+3} \end{array} \right|^\dagger \left(\begin{array}{cccc} \mathcal{T}_+ & \mathcal{Y}^- & \mathcal{X}^- & 0 \\ \mathcal{Y}^+ & \mathcal{T}_- & 0 & \mathcal{X}^- \\ \mathcal{X}^+ & 0 & \mathcal{T}_- & -\mathcal{Y}^- \\ 0 & \mathcal{X}^+ & -\mathcal{Y}^+ & \mathcal{T}_+ \end{array} \right) \left| \begin{array}{c} a_{1i} F_{m_h} \\ a_{2i} F_{m_h+1} \\ a_{3i} F_{m_h+2} \\ a_{4i} F_{m_h+3} \end{array} \right\rangle, \quad (19)$$

$$\begin{aligned}
\mathcal{T}_{\pm} &= - \left[A_L \left(\left[a(\Gamma_{15v}) \pm \frac{1}{2} b(\Gamma_{15v}) \right] \frac{\omega^2}{v_L^2} \mp \frac{3}{2} k_z^2 b(\Gamma_{15v}) \right) f_n(q_L r) \pm \frac{3}{2} A_{T_1} b(\Gamma_{15v}) k_z q_T f_n(q_T r) \right], \\
\mathcal{Y}^{\pm} &= \mp i \sqrt{3} b(\Gamma_{15v}) \left[A_L k_z q_L f_{n\pm 1}(q_L r) \mp \frac{1}{2} [A_{T_1} (q_T^2 - k_z^2) + A_{T_2} k_z q_T] f_{n\pm 1}(q_T r) \right], \\
\mathcal{X}^{\pm} &= \frac{\sqrt{3}}{2} b(\Gamma_{15v}) [A_L q_L^2 f_{n\pm 2}(q_L r) + (A_{T_1} k_z q_T - A_{T_2} q_T^2) f_{n\pm 2}(q_T r)]. \tag{20}
\end{aligned}$$

From Eqs. (18), (20) and the space of solution (7) we extract the following conclusions: a) For the phonon states with $n = 0$, $k_z = 0$ we have three independent hole-phonon interaction Hamiltonians, accounting for the three uncoupled subspaces, L , T_1 , T_2 , with eigenfrequencies ω_L , ω_{T_1} and ω_{T_2} , respectively. Evaluating (20) at $\omega = \omega_L$ and using the fact that $A_L \neq 0$ and $A_{T_1}, A_{T_2} = 0$, we see that the Hamiltonian (18) couples the diagonal intraband hole states $|i\rangle \Rightarrow |i\rangle$ and the weak coupling interband between $|lh^{\pm}\rangle \Leftrightarrow |hh^{\mp}\rangle$ states; if we choose $\omega = \omega_{T_1}$ where $A_L, A_{T_2} = 0$ and $A_{T_1} \neq 0$, we are in presence of interband transitions $|lh^{\pm}\rangle \Leftrightarrow |hh^{\pm}\rangle$; and for $\omega = \omega_{T_2}$ with $A_L, A_{T_1} = 0$ and $A_{T_2} \neq 0$, results in the $|lh^{\mp}\rangle \Leftrightarrow |hh^{\pm}\rangle$, holes scattering. b) Fixing $n = 0$, with $k_z \neq 0$ we are in presence of two independent subspaces, $L - T_1$ and T_2 . The first one couples the L and T_1 motions, while the second correspond to pure T_2 transverse phonon. Similar expressions are obtained for homogeneous wire by choosing properly the function $F_{m_h}(r)$ and $f_n(r)$ inside the cylinder.

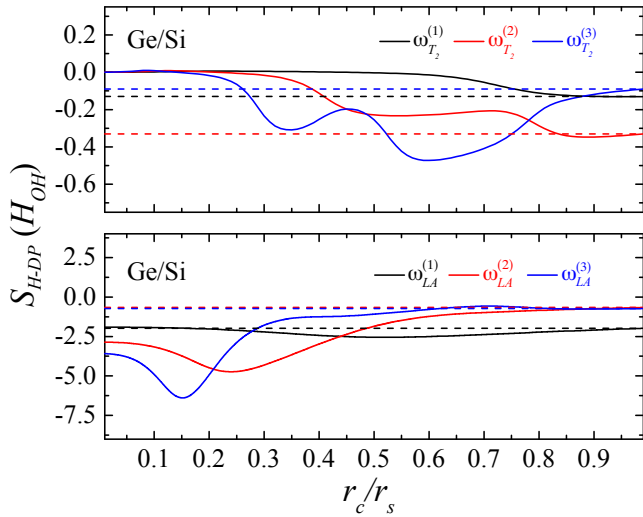


FIG. 7. (Color online) Reduced valence band scattering amplitude S_{H-BP}/H_{OH} for Ge/Si NWs as a function of the ratio r_c/r_s . For $k_z = 0$ and $n = 0$, the two sets of independent subspaces are displayed (see text): Upper panel transverse phonons with frequencies, $\omega_{T_2}^{(j)}$; lower panel longitudinal modes and frequencies $\omega_{LA}^{(j)}$ ($j = 1, 2, 3$). Dashed lines: homogeneous Ge nanowire.

In the size-quantum-limit and not to large value of k_z , the LK Hamiltonian splits into two independent 2×2 matrix, coupling ($|hh^+\rangle$, $|lh^-\rangle$) or ($|hh^-\rangle$, $|lh^+\rangle$) Bloch states (see Appendix C). For $k_z = 0$ and angular momentum quantum number $n = 0$, the scattering amplitude (19) splits into two independent terms, which correspond to the subspaces L and T_2 of the hole-phonon interaction Hamiltonian.

Figure 7 is devoted the hole scattering amplitude (19) for the first three T_2 transverse modes (upper panel) and three LA longitudinal modes (lower panel) of the Ge/Si structure as function of the ratio r_c/r_s . In the calculation we assumed that the lower hole state are completely confined in the core (hard wall potential approximation). As in Fig. 6 dashed lines represent the form factor but in this case for the Ge nanowire with a radius of 5 nm and S_{H-BP} measured in units of $H_{OH} = -a(\Gamma_{15v})\sqrt{\hbar\omega_{n=0}(k_z=0)/4\pi r_c^2 L \rho_c v_L^2}$ for each phonon mode. Here, the influence of the shell is solely due to Ge/Si phonon spectrum. From the figure we observe that S_{H-BP} for the longitudinal modes are one order of magnitude greater than the transverse ones, a fact that reflects the coupling between the hole states. In the case of T_2 we have a coupling between $|hh\rangle$ and $|lh\rangle$, while for the LA we are in presence of the diagonal components $|hh\rangle \rightarrow |hh\rangle$ and $|lh\rangle \rightarrow |lh\rangle$. Another feature is the strong oscillation of the S_{H-BP} for transverse modes with respect to the LA phonons. The T_2 vibrations couple the cylindrical function of second order, while for the LA modes, S_{H-BP} are proportional to the Bessel function J_0 . Also, a useful result can be extracted from the Fig. 7, that is, we can obtain the minimum value of r_c/r_s where hole-phonon Hamiltonian for core/shell NWs can be considered as a pure Ge wire. Notice that this result depend on the type of interaction, for LA $r_c/r_s \geq 0.6$ and for T_2 modes $r_c/r_s \geq 0.8$.

V. CONCLUSION

In summary, we have study the acoustical phonon dispersion, the vector phonon displacement and the electron- and hole-acoustical phonon Hamiltonians in core/shell Ge/Si and Si/Ge NWs. Our results show the influence of the coated Si-Ge based nanowires on the phonon frequencies and electron-phonon Hamiltonian. Due to the presence of the shell, the phonon frequencies exhibit oscillations as function of the ratio r_c/r_s leading

to a strong influence on the interaction Hamiltonians and scattering amplitudes. The gapless phonons have a tuned renormalized group sound velocities in terms of the geometrical factor r_c/r_s . Also, it is shown that scattering amplitudes for the conduction and valence bands can be handled by the size of the shell thickness. The obtained results are view as a basic tool and exploration of electron and hole transport phenomena and Brillouin light scattering as well as for device applications of these one-dimensional Ge/Si and Si/Ge core/shell nanostructures. The systematic deduction and explicit solutions, are relatively simple, of the electron and Bir-Pikus hole deformation potential Hamiltonians incorporating the characteristics of the phonon modes for the wavenumber $k_z = 0$, present straight applications to the resonant Raman scattering processes in core/shell NWs. Looking at different scattering configurations with respect to the axis of the cylinder, allows one to study the properties of the confinement phonons (LA and T_2 modes) in particular their dependence on the spatial confinement and intrinsic stress at the interface.

Appendix A: Stress tensor

For Ge and Si semiconductors with diamond structure, the relation between stress and strain, $\sigma = \mathbf{C} \cdot \boldsymbol{\varepsilon}$, in cylindrical coordinates, $\mathbf{r} = (r, \theta, z)$ can be written as

$$\begin{pmatrix} \sigma_{rr} \\ \sigma_{\theta\theta} \\ \sigma_{zz} \\ \sigma_{r\theta} \\ \sigma_{rz} \\ \sigma_{\theta z} \end{pmatrix} = \begin{pmatrix} C_{11} & C_{12} & C_{12} & 0 & 0 & 0 \\ C_{12} & C_{11} & C_{12} & 0 & 0 & 0 \\ C_{12} & C_{12} & C_{11} & 0 & 0 & 0 \\ 0 & 0 & 0 & C_{44} & 0 & 0 \\ 0 & 0 & 0 & 0 & C_{44} & 0 \\ 0 & 0 & 0 & 0 & 0 & C_{44} \end{pmatrix} \begin{pmatrix} \varepsilon_{rr} \\ \varepsilon_{\theta\theta} \\ \varepsilon_{zz} \\ 2\varepsilon_{r\theta} \\ 2\varepsilon_{rz} \\ 2\varepsilon_{\theta z} \end{pmatrix}, \quad (A1)$$

where the C_{ij} are the elastic stiffness coefficients and the components of the strain tensor in terms of the vector phonon displacement $\mathbf{u} = (u_r, u_\theta, u_z)$ are given by

$$\begin{aligned} \varepsilon_{rr} &= \frac{\partial u_r}{\partial r}; & \varepsilon_{\theta\theta} &= \frac{1}{r} \left(\frac{\partial u_\theta}{\partial \theta} + u_r \right); \\ \varepsilon_{zz} &= \frac{\partial u_z}{\partial z}, & \varepsilon_{r\theta} &= \frac{1}{2} \left(\frac{1}{r} \frac{\partial u_r}{\partial \theta} + \frac{\partial u_\theta}{\partial r} - \frac{u_\theta}{r} \right); \\ \varepsilon_{\theta z} &= \frac{1}{2} \left(\frac{\partial u_\theta}{\partial z} + \frac{1}{r} \frac{\partial u_z}{\partial \theta} \right); & \varepsilon_{rz} &= \frac{1}{2} \left(\frac{\partial u_r}{\partial z} + \frac{\partial u_z}{\partial r} \right). \end{aligned} \quad (A2)$$

Considering isotropic bulk materials the acoustic phonon branches at Γ are degenerate and we have that $C_{11} = \rho v_L^2$, $C_{44} = \rho v_T^2$ and $C_{12} = \rho v_L^2 - 2\rho v_T^2$ with $v_T(v_L)$ the transverse (longitudinal) sound velocity. Accordingly the stress tensor is reduced to

$$\sigma = \rho(v_L^2 - 2v_T^2)(\nabla \cdot \mathbf{u})\mathbf{I} + 2\rho v_T^2(\nabla \mathbf{u}),$$

where \mathbf{I} is the identity matrix.

Appendix B: Electron wave function

In the framework of the Envelope Function Approximation, the electron wave function $|\Psi_{\alpha_e}\rangle$ in cylindrical symmetry can be written as

$$\langle \mathbf{r} | \Psi_{\alpha_e} \rangle = \frac{1}{\sqrt{2V_c}} F_m(r) e^{i(m\theta + k_e z)}, \quad (B1)$$

where $V_c = \pi r_c^2 L$ is the core volume, $m\hbar$ ($m = 0, 1, 2, \dots$) and k_e are the z -component of the angular momentum and electron wave number, respectively and $F_m(r)$ the radial wave function. Considering bound states, we are in presence of two options:^{6,10}

a) Si/Ge nanowire, where the states are confined in the core. Hence, it is possible to show that

$$F_m(r) = \begin{cases} A_m^{(1)} J_m(p_c r); & 0 \leq r \leq r_c \\ A_m^{(2)} Q_{m,m}^-(|p_s| r); & r_c \leq r \leq r_s \end{cases}, \quad (B2)$$

with

$$Q_{m,n}^\pm(x) = I_m(x)K_n(\gamma x) \pm I_n(\gamma x)K_m(x),$$

$$A_m^{(1)} = \frac{1}{2} \frac{\sqrt{\mathcal{Q}_{m+1,m}^+ (|\tilde{p}_s|) \mathcal{Q}_{m-1,m}^+ (|\tilde{p}_s|)}}{\sqrt{J_{m+1}(\tilde{p}_c) J_{m-1}(\tilde{p}_c)}} \frac{\tilde{p}_s}{\tilde{p}_c} \mathcal{W}_m(|\tilde{p}_s|), \quad (B3)$$

$$A_m^{(2)} = \frac{1}{2} \mathcal{W}_m(|\tilde{p}_s|), \quad (B4)$$

and

$$\begin{aligned} \mathcal{W}_m(\tilde{p}_s) &= [\mathcal{Q}_{m+1,m}^-(|\tilde{p}_s|) \mathcal{Q}_{m-1,m}^-(|\tilde{p}_s|) - \\ &\quad \gamma^2 \mathcal{Q}_{m+1,m}^-(\gamma |\tilde{p}_s|) \mathcal{Q}_{m-1,m}^-(\gamma |\tilde{p}_s|) + \\ &\quad \mathcal{Q}_{m+1,m}^+ (|\tilde{p}_s|) \mathcal{Q}_{m-1,m}^+ (|\tilde{p}_s|) \frac{|\tilde{p}_s|^2}{\tilde{p}_c^2}]^{-\frac{1}{2}}. \end{aligned} \quad (B5)$$

b) In the case of Ge/Si core/shell, the electronic states are localized in the shell and the above equations are reduced to

$$F_m(r) = \begin{cases} A_m^{(1)} I_m(|p_c| r); & 0 \leq r \leq r_c \\ A_m^{(2)} \mathcal{P}_{m,m}(p_s r); & r_c \leq r \leq r_s \end{cases}, \quad (B6)$$

with the coefficients $A_m^{(i)}$ ($i = 1, 2$) equal to

$$A_m^{(1)} = \frac{1}{2} \frac{1}{\sqrt{I_{m+1}(|\tilde{p}_c|) I_{m-1}(|\tilde{p}_c|)}} \mathcal{R}_m(\tilde{p}_s), \quad (B7)$$

$$A_m^{(2)} = \frac{1}{2} \frac{1}{\sqrt{\mathcal{P}_{m+1,m}(\tilde{p}_s) \mathcal{P}_{m-1,m}(\tilde{p}_s)}} \frac{|\tilde{p}_c|}{\tilde{p}_s} \mathcal{R}_m(\tilde{p}_s), \quad (B8)$$

and

$$\mathcal{R}_m(\tilde{p}_s) = \left[1 - \frac{|\tilde{p}_c|^2}{\tilde{p}_s^2} \times \left(1 - \frac{4}{\pi^2 \tilde{p}_s^2} \frac{1}{\mathcal{P}_{m+1,m}(\tilde{p}_s) \mathcal{P}_{m-1,m}(\tilde{p}_s)} \right) \right]^{-\frac{1}{2}}.$$

As it is stated above $c(s)$ labels the core (shell) semiconductor and $p_c(p_s)$ is related with the electron energy by the equation

$$\bar{E}_e = \Delta E_g^{(c,s)} + \frac{\hbar^2 p_{c,s}^2}{2m_t^{(c,s)}} + \frac{\hbar^2 k_e^2}{2m_l^{(c,s)}}, \quad (\text{B9})$$

with $\tilde{p}_c(\tilde{p}_s) = p_c r_c(p_s r_c)$ and m_l (m_t) the longitudinal (transverse) conduction electron mass in the Γ point of the Brillouin zone. In Eq. (B9) $\bar{E}_e = E_g^{(c,s)} - E_{\text{strained}}$ takes into account the gap energy correction due to the intrinsic strain at the interface^{53,54} and $\Delta E_g^{(c,s)}$ is the band offset between the core and shell measured from the bottom of the band. For NWs wroth along [110] growth direction the band gap $\Delta E_g^{(c,s)} \simeq 300$ meV.¹⁰ In our calculations we have assumed $\Delta E_g^{(c,s)}$ independent of γ .

There is a third option, here not considered, where both, p_c and p_s are real, and the radial wave function $F_m(r)$ presents an oscillatory behavior in both the core and shell part, which correspond to higher excited states of the core/shell NWs.

Appendix C: Hole wave function

For a description of the hole states in the valence band we consider the LK Hamiltonian model neglecting the coupling from the split-off band. This Hamiltonian provides a good description for heavy-hole and light-hole states and the coupling between them due to the Γ_{15v} degeneracy of valence bands in the Γ point. Along the [110] direction and assuming the axial approximation, $\gamma_2 \simeq \gamma_3$, the 4×4 Hamiltonian can be written as^{51,55}

$$H_{LK} = \frac{\hbar^2}{m_0} \begin{pmatrix} D_{hh} & A_- & B_- & 0 \\ A_-^* & D_{lh} & 0 & B_- \\ B_-^* & 0 & D_{lh} & A_+^* \\ 0 & B_-^* & A_+ & D_{hh} \end{pmatrix}, \quad (\text{C1})$$

where

$$\begin{aligned} D_{hh} &= -\frac{(\gamma_1 + \gamma_s)}{2} \{ \hat{k}_+, \hat{k}_- \} - \frac{(\gamma_1 - 2\gamma_s)}{2} \hat{k}_h^2, \quad (\text{C2}) \\ D_{lh} &= -\frac{(\gamma_1 - \gamma_s)}{2} \{ \hat{k}_+, \hat{k}_- \} - \frac{(\gamma_1 + 2\gamma_s)}{2} \hat{k}_h^2, \\ A_{\pm} &= \mp\sqrt{3} \hat{\gamma} \hat{k}_{\pm} \hat{k}_h; \quad B_{\pm} = -\frac{\sqrt{3}}{2} \gamma_t \hat{k}_{\pm}^2, \end{aligned}$$

$\hat{\gamma} = (\gamma_2 + \gamma_3)/2$, $\gamma_s = (\gamma_2 + 3\gamma_3)/4$, $\gamma_t = (3\gamma_2 + 5\gamma_3)/8$, γ_1 , γ_2 and γ_3 are the Luttinger parameters. The total Hamiltonian for the valence band can be cast as $H = H_{LK} + V(r)$ with $V(r)$ the NWs confinement potential. The wave function $\langle \mathbf{r} | \Psi_{\alpha_h} \rangle$, as given by Eq. (B1), represents a basis for the effective 4×4 LK-Hamiltonian. Since the Bloch states, $|hh^+\rangle$, $|lh^+\rangle$, $|lh^-\rangle$ and $|hh^-\rangle$ are mixed by the effects of the cylindrical symmetry and the non-zero matrix elements A_{\pm} and B_{\pm} in Eq. (C2), we can write the general solution of the wave function $\langle \mathbf{r} | \Psi_{\alpha_h} \rangle$ with a special sequence of the angular quantum number m for each hole state. Thus, by exploring the symmetry of the Hamiltonian (C1), the exact wave function for the hole state $\langle \mathbf{r} | \Psi_{\alpha_h} \rangle$ can be written as

$$\langle \mathbf{r} | \Psi_{\alpha_h}^{(i)} \rangle = \widehat{F}_m^{(i)}(r) e^{i(m\theta + k_h z)} = \begin{pmatrix} a_{1i} F_m(p_{hh}) |hh^+\rangle \\ a_{2i} F_{m+1}(p_{hl}) e^{i\theta} |lh^+\rangle \\ a_{3i} F_{m+2}(p_{hl}) e^{2i\theta} |lh^-\rangle \\ a_{4i} F_{m+3}(p_{hh}) e^{3i\theta} |hh^-\rangle \end{pmatrix} e^{i(m\theta + k_h z)}, \quad (\text{C3})$$

where $p_{hh(lh)}$ is related with the heavy (light) hole energy by the expression

$$\bar{E}_{hh(lh)} = -\Delta E_g^{(c,s)} - \frac{\hbar^2}{2m_{hh(lh)}} (p_{hh(lh)}^2 + k_h^2), \quad (\text{C4})$$

and $m_{hh(lh)} = 1/(\gamma_1 - (+)2\gamma_s)$. As in the case of the conduction band in $E_{hh(lh)}$ we consider the band gap correction. The vector coefficients $\mathbf{a}_i |i\rangle$ ($i = hh^+, lh^+, lh^-, hh^-$) in (C3) are⁵⁶

$$\begin{aligned} \mathbf{a}_{hh^+}^{\dagger} &= a_{hh^+} \left(-\frac{1}{\sqrt{3}} \left(1 + \frac{4k_h^2}{p_{hh}^2} \right), -\frac{2k_h}{p_{hh}}, 1, 0 \right), \\ \mathbf{a}_{lh^+}^{\dagger} &= a_{lh^+} \left(-\sqrt{3}, -\frac{2k_h}{p_{lh}}, 1, 0 \right), \\ \mathbf{a}_{lh^-}^{\dagger} &= a_{lh^-} \left(-\frac{2k_h}{p_{lh}}, \frac{1}{\sqrt{3}} \left(1 + \frac{4k_h^2}{p_{lh}^2} \right), 0, 1 \right), \\ \mathbf{a}_{hh^-}^{\dagger} &= a_{hh^-} \left(-\frac{2k_h}{p_{hh}}, -\sqrt{3}, 0, 1 \right), \end{aligned}$$

where the wight coefficients a_{hh^+} , a_{lh^+} , a_{lh^-} , a_{hh^-} give a measure of the mixtures of Bloch states $|i\rangle = |hh^+\rangle$, $|lh^+\rangle$, $|lh^-\rangle$ and $|hh^-\rangle$. Imposing continuity of the wave function $\langle \mathbf{r} | \Psi_{\alpha_h}^{(i)} \rangle$ and its derivative at the core/shell interface $r = r_c$ and choosing the boundary condition $\langle \mathbf{r} | \Psi_{\alpha_h}^{(i)} \rangle |_{r=r_s} = 0$ we find the normalized eigensolutions and eigenenergies for the hole states.

In the case of Ge/Si core/shell nanowires, the hole are mostly confined in the core and the valence band offset is of the order 0.5 eV.^{6,10,57} Thus, in the limit of strong spatial confinement we can assume a hard wall potential and the holes are completely confined in the core.

In the evaluation of the hole energy and wave function we employed for Si[Ge] the values $\gamma_1 = 4.22[13.4]$, $\gamma_2 =$

0.39[4.24], $\gamma_3 = 1.44[5.69]$, $a(\Gamma_{15v}) = -5.0[-5.2]$ eV and $b(\Gamma_{8v}) = -2.3[-2.4]$ eV.⁴⁹

ACKNOWLEDGMENTS

D. S-P, C. T-G and G. E. M acknowledge support from the Brazilian Agencies FAPESP (processes: 2015/23619-

1, 2014/19142-2) and CNPq.

¹ A. Khitun, A. Balandin, and K. Wang, *Superlattices and Microstructures* **26**, 181 (1999).

² P. Servati, A. Colli, S. Hofmann, Y. Fu, P. Beecher, Z. Durran, A. Ferrari, A. Flewitt, J. Robertson, and W. Milne, *Physica E: Low-dimensional Systems and Nanostructures* **38**, 64 (2007).

³ B. Tian, X. Zheng, T. J. Kempa, Y. Fang, N. Yu, G. Yu, J. Huang, and C. M. Lieber, *Nature* **449**, 885 (2007).

⁴ F. Murphy-Armando, G. Fagas, and J. C. Greer, *Nano Letters* **10**, 869 (2010).

⁵ A. I. Hochbaum, R. Fan, R. He, and P. Yang, *Nano Letters* **5**, 457 (2005).

⁶ X. Peng and P. Logan, *Applied Physics Letters* **96**, 143119 (2010).

⁷ M. C. Wingert, Z. C. Y. Chen, E. Dechaumphai, J. Moon, J.-H. Kim, J. Xiang, and R. Chen, *Nano Letters* **11**, 5507 (2011).

⁸ M. Hu, K. P. Giapis, J. V. Goicochea, X. Zhang, and D. Poulikakos, *Nano Letters* **11**, 618 (2011).

⁹ M. Amato, M. Palummo, R. Rinaldi, and S. Ossicini, *Chemical Reviews* **114**, 1371 (2014).

¹⁰ L. Yang, R. N. Musin, X.-Q. Wang, and M. Y. Chou, *Phys. Rev. B* **77**, 195325 (2008).

¹¹ X. Peng, F. Tang, and P. Logan, *Journal of Physics: Condensed Matter* **23**, 115502 (2011).

¹² S. Huang and L. Yang, *Applied Physics Letters* **98**, 093114 (2011).

¹³ R. Kagimura, R. W. Nunes, and H. Chacham, *Phys. Rev. Lett.* **98**, 026801 (2007).

¹⁴ P. Logan and X. Peng, *Phys. Rev. B* **80**, 115322 (2009).

¹⁵ X. Zhao, C. M. Wei, L. Yang, and M. Y. Chou, *Phys. Rev. Lett.* **92**, 236805 (2004).

¹⁶ S. P. Beckman, J. Han, and J. R. Chelikowsky, *Phys. Rev. B* **74**, 165314 (2006).

¹⁷ D. Medaboina, V. Gade, S. K. R. Patil, and S. V. Khare, *Phys. Rev. B* **76**, 205327 (2007).

¹⁸ E. Pokatilov, D. Nika, and A. Balandin, *Superlattices and Microstructures* **38**, 168 (2005).

¹⁹ R. Yang, G. Chen, and M. S. Dresselhaus, *Nano Letters* **5**, 1111 (2005).

²⁰ J. Chen, G. Zhang, and B. Li, *Nano Letters* **12**, 2826 (2012).

²¹ N. Neophytou and H. Kosina, *Nano Letters* **10**, 4913 (2010).

²² I. M. Tienda-Luna, F. G. Ruiz, A. Godoy, L. Donetti, C. Martnez-Blanque, and F. Gmiz, *Applied Physics Letters* **103**, 163107 (2013).

²³ J. Treu, M. Bormann, H. Schmeiduch, M. Dblinger, S. Morktter, S. Matich, P. Wiecha, K. Saller, B. Mayer, M. Bichler, M.-C. Amann, J. J. Finley, G. Abstreiter, and G. Koblmller, *Nano Letters* **13**, 6070 (2013).

²⁴ B. Mayer, D. Rudolph, J. Schnell, S. Morkötter, J. Winerl, J. Treu, K. Müller, G. Bracher, G. Abstreiter, G. Koblmüller, and J. J. Finley, *Nature Communications* **4** (2013).

²⁵ Y. Hu, F. Kuemmeth, C. M. Lieber, and C. M. Marcus, *Nature Nanotech* **7**, 47 (2011).

²⁶ A. P. Higginbotham, T. W. Larsen, J. Yao, H. Yan, C. M. Lieber, C. M. Marcus, and F. Kuemmeth, *Nano Letters* **14**, 3582 (2014).

²⁷ P. B. Peelaers, H. and F. Peeters, *Acta Physica Polonica A* **122**, 294 (2012).

²⁸ H. Peelaers, B. Partoens, and F. M. Peeters, *Phys. Rev. B* **82**, 113411 (2010).

²⁹ G.-Y. Huang and Y.-L. Kang, *Journal of Applied Physics* **110**, 023526 (2011).

³⁰ C. Kloeffel, M. Trif, and D. Loss, *Phys. Rev. B* **90**, 115419 (2014).

³¹ J. Hattori, S. Uno, N. Mori, and K. Nakazato, *Mathematical and Computer Modelling* **51**, 880 (2010).

³² A. K. Buin, A. Verma, and M. P. Anantram, *Journal of Applied Physics* **104**, 053716 (2008).

³³ S. Yu, K. W. Kim, M. A. Stroscio, and G. J. Iafrate, *Phys. Rev. B* **51**, 4695 (1995).

³⁴ O. Madelung, *Introduction to Solid State Theory* (Springer, 1996).

³⁵ P. Y. Yu and M. Cardona, *Fundamentals of Semiconductors: Physics and Materials Properties* (Springer, 2010).

³⁶ J. T. Arantes and A. Fazzio, *Nanotechnology* **18**, 295706 (2007).

³⁷ X. Peng, F. Tang, and P. Logan, *Journal of Physics: Condensed Matter* **23**, 115502 (2011).

³⁸ G. Bir and G. Pikus, *Symmetry and Strain-induced Effects in Semiconductors*, A Halsted press book (Wiley, New York, 1974).

³⁹ It is established that the values of deformation potentials are modified by the orientation and the spatial confinement. In a first approach we are choosing the bulk values Ref. 4.

⁴⁰ M. Born and K. Huang, *Dynamical Theory of Crystal Lattices* (Clarendon Press, Oxford, 1988).

⁴¹ C. Trallero-Giner, R. Pérez-Álvarez, and F. García-Moliner, *Long wave polar modes in semiconductor heterostructures*, 1st ed. (Pergamon Elsevier Science, London, 1998).

⁴² D. G. Santiago-Pérez, C. Trallero-Giner, R. Pérez-Álvarez, L. Chico, and G. E. Marques, *Phys. Rev. B* **91**, 075312 (2015).

⁴³ M. Abramowitz and I. Stegun, *Handbook of Mathematical Functions* (U. S. Goverment Printing Office, Whashinton, D. C, 1964).

⁴⁴ J. Maultzsch, H. Telg, S. Reich, and C. Thomsen, Phys. Rev. B **72**, 205438 (2005).

⁴⁵ J. Kürti, V. Zólyomi, M. Kertesz, and S. Guangyu, New Journal of Physics **5**, 125 (2003).

⁴⁶ E. Bourgeois, M.-V. Fernández-Serra, and X. Blase, Phys. Rev. B **81**, 193410 (2010).

⁴⁷ A. Trejo, R. Vazquez-Medina, G. Duchen, and M. Cruz-Irisson, Physica E: Low-dimensional Systems and Nanostuctures **51**, 10 (2013).

⁴⁸ Along the [011] crystallographic direction the transversal phonon velocity are no degenerated with $v_{T_1} = 5.84[3.84] \times 10^5 \text{ cm/s}$ $v_{T_2} = 4.67[2.76] \times 10^5 \text{ cm/s}$ for Si[Ge]. We employed the average values $v_T = (v_{T_1} + v_{T_2})/2$.

⁴⁹ S. Adachi, *Properties of Group-IV, III-V and II-VI Semiconductors* (John Wiley and Sons, Chichester, 2005).

⁵⁰ E. B. Ramayya, D. Vasileska, S. M. Goodnick, and I. Knezevic, Journal of Applied Physics **104**, 063711 (2008).

⁵¹ J. M. Luttinger, Phys. Rev. **102**, 1030 (1956).

⁵² C. Kloeffel, M. Trif, and D. Loss, Phys. Rev. B **84**, 195314 (2011).

⁵³ C. Herring and E. Vogt, Phys. Rev. **101**, 944 (1956).

⁵⁴ Y. Sun, S. E. Thompson, and T. Nishida, Journal of Applied Physics **101**, 104503 (2007).

⁵⁵ J. M. Luttinger and W. Kohn, Phys. Rev. **97**, 869 (1955).

⁵⁶ P. C. Sercel and K. J. Vahala, Phys. Rev. B **42**, 3690 (1990).

⁵⁷ J.-S. Park, B. Ryu, C.-Y. Moon, and K. J. Chang, Nano Letters **10**, 116 (2010).